Journal of Applied Research and Technology

www.jart.icat.unam.mx

ICAT Instituto de Ciencias Aplicadas y Tecnología

Journal of Applied Research and Technology 24 (2026) 704-717

Original

Wear Performance of Tungsten Carbide-Nickel-Chromium Coating Produced by Laser Cladding

Gabriel Viana Figueiredo[1] • Germán Alberto Barragán de los Rios[2*]
Patricia Fernández-Morales[3] • Fábio Edson Mariani[1]
Luiz Carlos Casteletti[1] • Reginaldo Teixeira Coelho[1]

[1]University of São Paulo/São Carlos, School of Engineering, São Paulo, Brazil
[2]Grupo de investigación en Ingeniería Aeroespacial, Universidad Pontificia Bolivariana, Medellín, Colombia
[3]Grupo de investigación en Nuevos Materiales, Universidad Pontificia Bolivariana, Medellín, Colombia

Abstract: The manufacturing of end-use parts and high-volume production tooling, such as molds and dies, presents distinct challenges regarding dimensional accuracy, flexibility, and production speed. Laser cladding has emerged as a promising technique, offering high energy density, low elemental dilution, and minimal thermal damage to substrates, making it ideal for producing dense, well-bonded coatings. By optimizing laser cladding parameters, remanufactured surfaces can be generated with superior properties compared to the original, uncoated parts. This study focuses on the characterization of WC-7Ni-19Cr coatings applied to AISI H13 and AISI 4140 steels, which are representative of injection mold materials and blades used in steam turbine energy generation from sugarcane bagasse combustion, respectively. The coatings were evaluated to identify optimal cladding parameters and were characterized using laser confocal microscopy, Vickers microhardness testing, and microadhesive wear analysis. The results demonstrated that the coatings were homogeneous, exhibited high hardness and wear resistance, and outperformed the respective substrates. These findings highlight the potential for laser cladding in enhancing industrial component performance.

Keywords: **Laser cladding, AISI H13, AISI 4140, WC-7Ni-19Cr, coatings, microadhesive wear tests.**

*Corresponding author.
E-mail address: german.barragan@upb.edu.co (A.A.J. Al Noor).
Peer Review under the responsibility of Universidad Nacional Autónoma de México.

1. Introduction

Coatings play a vital role, particularly in industrial applications, where they help extend the lifespan of mechanical components exposed to harsh oxidizing or abrasive conditions (Chen et al., 2022; John et al., 2022; (Posmyk & Myalski, 2023). Given the wide variety of industrial needs, numerous coating processes have been developed to meet specific demands (Fotovvati et al., 2019; Abijith et al., 2018). In recent decades, the rapid advancement of laser technology has enabled the creation of high-quality material coatings (John et al., 2022). Laser cladding, an advanced surface modification technique, uses a high-energy-density laser beam to fuse cladding materials with the substrate surface, forming a protective filler layer (Santo, 2008). This process is characterized by its rapid melting and cooling (Han et al., 2022), which promotes metallurgical bonding (Ahn, 2021) between the feedstock and the substrate while minimizing deformation (Svetlizky et al., 2021). Laser cladding, classified under additive manufacturing (AM) as a directed energy deposition (DED) process in ASTM and ISO standards (Dasgupta & Dutta, 2022), involves complex laser-material interactions and intricate metallurgical and physicochemical reactions (Ghosal et al., 2018; Toyserkani et al., 2017). These interactions are directly influenced by process parameters, which determine the quality and characteristics of the coating (Shamsaei et al., 2015; Thompson et al., 2015). Various applications of laser cladding coatings have been studied (Birger et al., 2011; Gong et al., 2023; John et al., 2022), with research often focusing on process variables (Sun et al., 2022; You et al., 2023), performance outcomes (Han et al., 2022), or both. There is broad agreement that the choice of cladding material is crucial for ensuring coating quality and effectiveness.

While many materials are compatible with additive manufacturing, metal applications deserve special attention as they represent the most significant and widely used sectors. (Armstrong et al., 2022; Cooke et al., 2020). One of the key challenges in metal additive manufacturing is understanding material behavior during thermal cycles, which involve rapid solidification, directional cooling, and phase transformations (Kirka et al., 2017; Singh et al., 2017). These factors introduce complexities in analyzing microstructural evolution and material properties that differ significantly from those in conventional processes (Shamsaei et al., 2015; Thompson et al., 2015). Among the various coating options, metal matrix composites reinforced with hard ceramic particles, such as tungsten carbide (WC), are commonly used (St-Georges, 2007). WC exhibits high wettability with metal alloys, such as nickel (Ni) and cobalt (Co), which is essential for forming high-quality composites. In WC-based composites, the matrix typically consists of metals with lower melting points, such as Co, Fe, and Ni, with Cr sometimes added to enhance corrosion resistance (Matthews et al., 2021a; Tougherghi et al., 2022; Wang et al., 2022).

The WC-Ni-Cr composite material, composed of tungsten carbide particles dispersed within a nickel-chromium matrix, offers a combination of high hardness, chemical and thermal stability (from WC particles), and toughness, impact resistance, and excellent corrosion resistance (from the Ni-Cr matrix) (Matthews et al., 2021b; Van Acker et al., 2005). The overall performance of the material is influenced by its composition, microstructure, and processing parameters, all of which can be tailored to meet specific application requirements (Oladijo et al., 2014). Key factors such as substrate dilution rate, surface quality, geometric accuracy, and mechanical properties are significantly affected by the cladding process parameters (You et al., 2023; Dong & Fan, 2015; Sun et al., 2022).

Given that 70–80 % of mechanical equipment failures are attributed to cumulative wear (Han et al., 2022; John et al., 2022), understanding and improving the wear resistance of components is a critical area of research. This paper investigates the hardness and wear behavior of a WC-7Ni-19Cr coating applied via laser cladding to substrates used in high-wear environments where durability is crucial. This particular combination of coating, substrate material, and cladding technique has not been extensively documented in the literature, and the results offer promising insights for future applications.

2. Materials and Methods

2.1 Materials

Two distinct steel sheets, AISI 4140 and AISI H13, were utilized as test substrates in this experiment. The selection of these materials was based on their unique processing and mechanical properties, making them suitable for diverse applications. AISI 4140 steel is renowned for its versatility, commonly used in manufacturing axles, shafts, and gears. In contrast, AISI H13 is widely employed in producing hot work tooling for die casting, extrusion, and forging applications. All substrate sheets maintained a uniform thickness of 5 mm, a dimension chosen based on preliminary tests that indicated it was optimal for minimizing distortion caused by thermal stresses. The rationale for selecting these specific substrate materials stems from their excellent wear resistance, aligning perfectly with

the requirements of their respective application areas. Despite intrinsic differences in chemical composition and mechanical characteristics, the selected substrates enable a comparative investigation into the coating process's effectiveness across various operational scenarios.

The substrates were heat-treated according to the conditions outlined in Table 1. During the austempering procedure, two distinct temperature thresholds were carefully established, guided by a thorough literature review (Borchers et al., 2020; Du et al., 2023) and previous research experiences (Edson Mariani et al., 2023). This approach ensured a thoughtful integration of relevant material properties and desired outcomes. The samples underwent meticulously planned isothermal quenching processes using oil-based media, aimed at achieving a specific microstructural configuration that imparts enhanced mechanical properties and wear resistance. One inherent advantage of the austempering process is its ability to facilitate slow cooling rates, which reduces the risk of distortion and fracture—key concerns in material processing. As a result, the specimens exhibit improved performance profiles during operational deployment, benefiting from these advantageous cooling kinetics.

Table 1. Substrates heat treatment conditions.

Material	Austenization		Quenching Medium	Tempering	
	°C	Time		°C	Time
AISI 4140	870	4 hours	Oil	200	1 hour
AISI H13	1030	4 hours	Oil	540	2 hours

The treatment parameters for various materials are critical to achieving optimal properties. For AISI 4140, austenitizing at 870 °C for 4 hours is within the recommended range, allowing for the dissolution of carbides and formation of a homogeneous structure. This is essential for effective quenching and heat treatment. Oil quenching provides fast yet controlled cooling, minimizing deformation and fractures. Tempering at 200 °C for 1 hour reduces brittleness without significant loss of hardness. However, tempering temperature may vary based on the material's final use, with higher temperatures sometimes used to enhance hardness.

Austenitizing AISI H13 at 1030 °C for 4 hours is ideal for this high-alloy steel, commonly used in hot-working tools. This temperature ensures the complete dissolution of carbides, resulting in a homogeneous microstructure that enhances wear resistance and thermal stability. Oil quenching is necessary to prevent the formation of soft or brittle structures, which would reduce wear resistance.

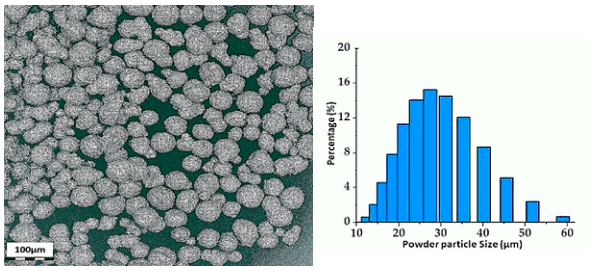

Figure 1. WC-7Ni-19Cr powder confocal image.

Tempering at 540 °C for 2 hours improves both hardness and wear resistance, maintaining a balance between hardness and toughness, crucial for applications such as forging dies and high-temperature casting.

While the heat treatment parameters for AISI 4140 and AISI H13 were standardized to optimize mechanical properties like wear resistance, the study did not directly measure or report hardness values. The primary focus was on the impact of the cladding process on the components' properties.

The cladding material used in this study was a commercially available WC-7Ni-19Cr powder. The structural characteristics of the powder were meticulously examined using a confocal microscope. Figure 1 presents the confocal image of the powder along with its particle size distribution.

The powder used for cladding has a size distribution ranging from 15 to 45 µm, and the figure clearly shows that the predominant particle geometries are spherical, although some irregularities in morphology are present, along with a minimal occurrence of satellite formation. The selection of the cladding material was based on its exceptional hardness and wear resistance properties, making it ideal for use as a protective layer on components that require resistance to abrasive particles, hard surfaces, fretting, particle erosion, and wear in various environmental conditions.

2.2 Cladding Procedure

WC-7Ni-19Cr powder was used as the coating material and applied via a pre-placed cladding technique (see Figure 2). In this method, the powder is initially distributed over the substrate. However, maintaining the particles in position until melting can be challenging and costly due to machine limitations and gas flow interactions. To overcome this issue, a sludge mixture consisting of the powder and a polyvinyl acetate (PVA) polymer solution in a 1:1 ratio was utilized. The sludge was applied to the substrate and dried at 150 °C for 20 minutes to facilitate water evaporation and curing.

PVA, commonly used as a binder in powder metallurgy and additive manufacturing, helps stabilize the powder during the pre-cladding stage. During rapid heating—particularly in laser cladding—intense thermal gradients promote its quick evaporation. Based on previous tests, the range of laser power employed in this study guarantees the complete evaporation of PVA during processing, thereby preventing the formation of gas pockets, voids, or other defects in the final coating.

The preplaced technique offers significant advantages, particularly in optimizing powder utilization and reducing wear on the machine, especially on the components of the deposition head, which are prone to damage when using coarse powders. This variation of the cladding process has been previously employed and described by da Silva et al. (2023). To ensure the even distribution of the mixture of powder and polyvinyl acetate (PVA) polymer solution on the substrate surface, a mechanical method is employed to aid in achieving uniform application. This approach enhances the consistency of the coating, ensuring that the powder-polymer mixture is evenly spread across the surface before the cladding process begins.

The BeAM® Modulo 250 machine was employed as the energy source for this experiment. This directed energy deposition (DED) machine is equipped with a coaxial Nd laser focused 3.5 mm above the surface to create a 0.8 mm spot size, featuring a top hat energy distribution and controlled by a Siemens® 840D CNC. To protect the optical system and the melt pool from contamination or oxidation, an argon flow of 12 L/min was directed through the deposition head. These parameters were selected based on previous successful coating operations performed with the same machine, as reported in (Barragan et al., 2021a; Edson Mariani et al., 2023), which achieved excellent fusion zones and optimal equipment protection.

Laser single tracks were produced by adjusting the laser power and travel speed. Two travel speeds, 300 and 500 mm/min, and three laser powers, 250, 350, and 450 W, were used, resulting in six different configurations for study. The choice of these parameters was based on preliminary tests and a review of the literature (G. Barragan et al., 2021b). The tracks were then analyzed to determine the most suitable parameters for coating, focusing on achieving strong adhesion without layer detachment, while minimizing the heat-affected zone (HAZ) to preserve the substrate properties. Additionally, appropriate dilution of the cladding material was critical—excessive dilution compromises the material's intrinsic properties, while insufficient dilution prevents a solid metallurgical bond with the substrate. The dilution rate of a laser track

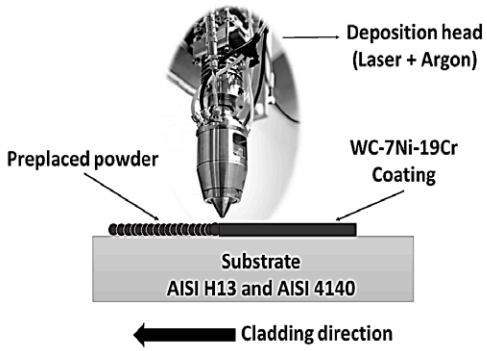

Figure 2. Schematic of preplaced powder cladding procedure.

was determined by measuring its cross-section. The process parameters yielding the best results were selected for coating a 35 mm x 35 mm area using a zigzag laser movement strategy with 33% overlap.

2.3 Metallographic Observation

To examine the cross-sectional regions, the samples were labeled and embedded for metallographic analysis. They were then polished and sanded using an alumina suspension (0.05 µm) and SiC sandpaper with progressively finer meshes: 80, 140, 220, 320, 400, 600, 1000, and 1200 grit. For microstructural observation, a chemical etching process was performed: AISI 4140 steel was etched with Villella's reagent (5 m HCl + 2 g picric acid + 100 ml ethyl alcohol) for 10 seconds, while AISI H13 steel was etched with Nital 2% (2 mL HNO_3 + 98 ml ethyl alcohol). After metallographic preparation, the coatings were examined using an Olympus® OLS4000 laser confocal microscope with an integrated camera.

2.4 Microhardness Tests

To measure the hardness of the generated substrates and coatings, Vickers microhardness (HV) tests were conducted using a Buhler® micro durometer, model 1600-6300, in accordance with the ASTM E384-17 standard. The tests utilized a load of 200 gf applied for 15 seconds. In addition to calculating the average hardness, micro-hardness profiles were established by taking a series of measurements at approximate intervals of 0.05 mm. These intervals were selected to ensure a uniform distribution of samples, covering the entire coating and extending to a significant depth of the substrate. This methodology facilitated the evaluation of how the surface property evolved toward the center of the substrate sample, as well as how the coating hardness varied with distance from the substrate surface.

2.5 Wear Test

The wear resistance of both the produced coatings and the substrates was evaluated using microadhesive wear tests as detailed in (Esteves et al., 2019). Figure 3 illustrates the schematic of the test machine utilized. The wear test machine was developed by the Department of Materials Engineering at the São Carlos School of Engineering, University of São Paulo. The specimens were sanded with sandpaper of various grits (80, 140, 220, 320, 400, 600, 800, 1000, and 1200 mesh) and polished using a 0.05 µm alumina suspension to obtain a smooth, interference-free surface suitable for micro-scale testing. A 1-inch steel ball made of AISI 52100, which was quenched and tempered to a hardness of 61 HRC, was employed for the tests. Each trial utilized a single test sphere at room temperature with a humidity level of 53%. The ball was meticulously cleaned before each test to prevent any potential contamination. Four tests were performed, varying in duration (5, 10, 15, and 20 minutes), under a load of 300 g (5.25 N) at a constant speed of 265 rpm.

For each sample, the test was conducted four times to determine the mean volume removed and the associated standard deviations. These parameters were specified to prevent any interfacial characteristics from influencing the microstructural properties during the experiments. Initially, the tested sections took on a cap-like shape, and their average diameters were used to calculate the worn volumes. The distances traveled and average volumes removed were calculated from the average diameters of the wear tracks created by the friction between the steel ball and the sample, as described in Equation 1.

$$V = (\pi.d\hat{}4)/(64.R)\ for\ d << R \quad (1)$$

Where V represents the removed volume, d is the average diameter of the produced cap, and R is the radius of the sphere.

3. Results

The initial depositions aimed to optimize the parameters for the selected material combination, WC-7Ni-19Cr coating, on two substrates: AISI 4140 and AISI H13. Since laser cladding involves melting and rapid solidification, it induces intense thermal cycles that can impact the structural integrity of the clad component due to significant thermal stresses between the coating and the substrate. These stresses may result in cracking, delamination, or deformation, adversely affecting the component's functional properties. A preliminary visual inspection of the coated samples revealed no visible defects, with the macroscopic properties being consistent and continuous, indicating an absence of surface flaws.

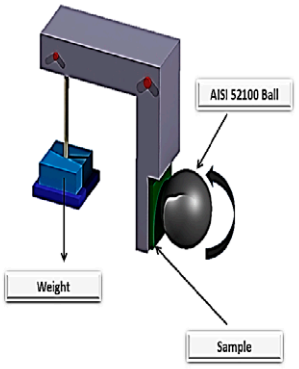

Figure 3. Test machine schematic.

The laser-clad coating can be divided into three distinct zones: the WC-7Ni-19Cr cladding layer, the heat-affected zone (HAZ), and the substrate. To assess the quality of the coating, cross-sectional profiling was performed to evaluate coating uniformity, the HAZ region, and dilution. Dilution is a critical factor in determining cladding quality, as the substrate inevitably dilutes the cladding material during the process. The surface of the substrate must melt to form a strong metallurgical bond at the interface. However, controlling dilution is essential to preserve the material properties of both the substrate and the cladding. In this study, the parameter configuration that achieved favorable coating properties with minimal dilution was deemed optimal. Optical images of transverse sections of the deposited layers of WC-7Ni-19Cr on the AISI 4140 substrate, along with their respective laser power and travel speed parameters (300 mm/min or 500 mm/min), are shown in Figures 4 to 6.

When laser cladding was performed at the lowest deposition speed of 300 mm/min with a laser power of 250 W, several notable issues became apparent in the resulting microstructure, as can be observed in the micrograph. This combination of parameters led to incomplete melting of the cladding material, primarily due to the low energy density provided by the laser. Insufficient energy caused poor wettability between the molten cladding and the substrate surface, which prevented a strong metallurgical bond from forming. As a result, significant irregularities, such as pores, were visible in the deposited layer, and in some regions, no deposition occurred at all. This lack of uniformity highlights the challenges of achieving proper material fusion at lower power and speed, which can severely impact the mechanical integrity of the coating.

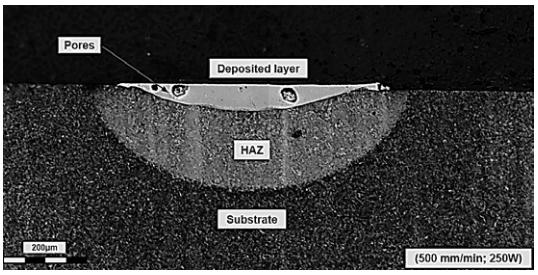

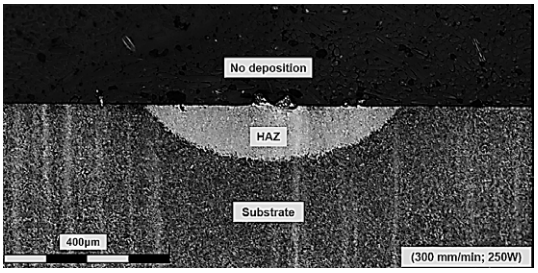

Figure 4. WC-7Ni-19Cr deposited on AISI 4140 steel substrate using a power of 250 W.

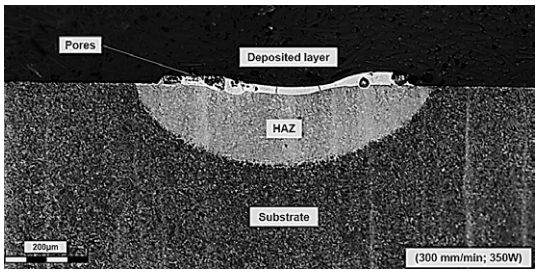

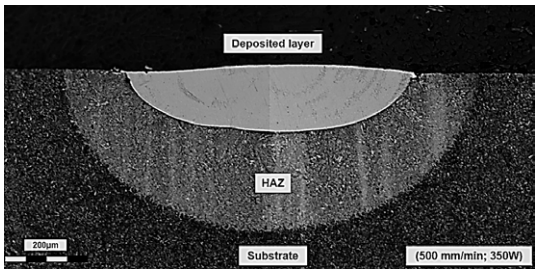

Figure 5. WC-7Ni-19Cr deposited on AISI 4140 steel substrate using a power of 350 W.

In contrast, when a higher deposition speed of 500 mm/min was combined with a laser power of 450 W, the amount of deposited material increased significantly. The cladding material fully melted and adhered to the substrate, producing a thicker and more continuous deposition layer. However, this improvement in deposition quality came at the cost of a significantly enlarged heat-affected zone (HAZ), as shown in the corresponding image. The HAZ represents the area of the substrate that underwent thermal alteration during the cladding process, which can lead to changes in the substrate's microstructure, such as grain growth or phase transformations. An excessively large HAZ is undesirable because it can weaken the substrate, particularly if it reduces toughness or alters the hardness of the steel. Additionally, at higher power levels, disturbances in the molten pool were more pronounced, leading to increased surface roughness, which could negatively affect the coating's tribological performance, such as wear resistance.

The microstructural observations at these different parameter combinations provide clear evidence of the trade-offs involved in laser cladding. For instance, at 300 mm/min and 250 W, the deposition layer showed visible pores and incomplete bonding, while at 500 mm/min and 450 W, the larger HAZ and rough surface texture indicated excessive heat input and molten pool turbulence. This highlights that while higher power can improve material melting and deposition uniformity, it can also introduce thermal stresses and surface defects that are detrimental to the overall coating quality.

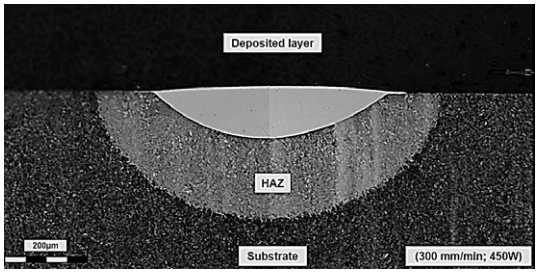

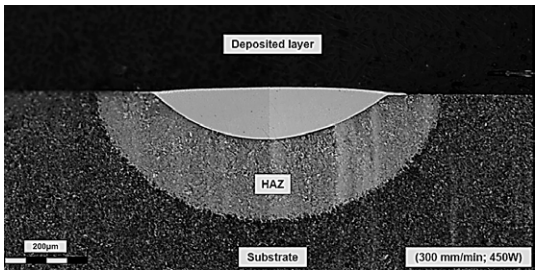

Figure 6. WC-7Ni-19Cr deposited on AISI 4140 steel substrate using a power of 450 W.

The most favorable configuration was found with a deposition speed of 500 mm/min and a lower laser power of 250 W. This combination yielded a relatively uniform and defect-free deposition layer, as seen in the micrograph, with minimal porosity and a controlled HAZ size. The reduced HAZ under these conditions minimized the thermal impact on the substrate, preserving its original microstructure while still allowing for sufficient melting and bonding of the cladding material. This suggests that a balance between laser power and speed is essential

for optimizing the coating's performance. By carefully adjusting the deposition parameters, it is possible to achieve a high-quality coating with a strong bond to the substrate, minimal defects, and limited alteration of the substrate's microstructure.

Overall, the images and analysis reveal the critical importance of optimizing the laser cladding parameters to achieve the best possible coating quality. At low power and speed, the deposition was inconsistent, with pores and incomplete melting. At high power, the coating improved in uniformity, but the excessive heat created a large HAZ and surface roughness. The optimal balance was found at 500 mm/min and 250 W, which provided good deposition with minimal thermal effects on the substrate, demonstrating the delicate interplay between energy input, deposition speed, and the resulting microstructure in laser cladding processes.

Figures 7 to 9 show the results of the process employing the same parameter combination over an AISI H13 steel substrate. Consistent magnification levels were employed during the image acquisition process to enable straightforward comparisons across all images of the deposition lines.

The laser cladding process on an AISI H13 steel substrate shows both similarities and notable differences compared to the previous results with the AISI 4140 substrate. As seen in Figure 7, irregular deposition is present at lower power and speed settings (300 mm/min and 250 W), similar to the results with AISI 4140. The insufficient energy density once again causes poor wettability and incomplete bonding between the cladding layer and the substrate, leading to defective coating formation. However, in the AISI H13 substrate, the irregularity of the deposition appears more pronounced, with rougher and more uneven features in the deposited material, possibly due to the different thermal conductivity or alloy composition of H13 steel, which could affect heat distribution and energy absorption.

At higher power and speed settings (e.g., 500 mm/min and 450 W), the heat-affected zone (HAZ) remains significant, as seen in both materials. The larger HAZ reflects the higher energy input, leading to deeper thermal penetration into the substrate, but here, the HAZ in AISI H13 appears slightly more controlled, with smoother transitions in the deposited layer compared to AISI 4140. Similarities include the overall trend of improved deposition thickness and layer uniformity at higher power levels, but with the trade-off of increased thermal impact on the substrate. Both materials exhibit relatively good deposition layers at higher power (350 W and 450 W), although surface roughness and porosity remain concerns at certain parameter combinations.

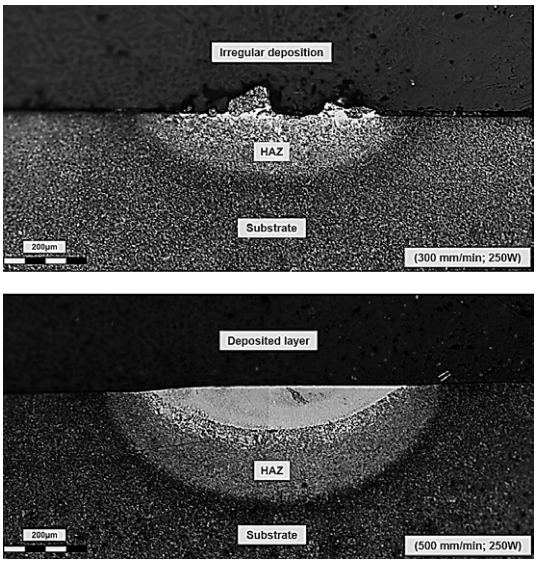

Figure 7. WC-7Ni-19Cr deposited on AISI H13 steel substrate using a power of 250 W.

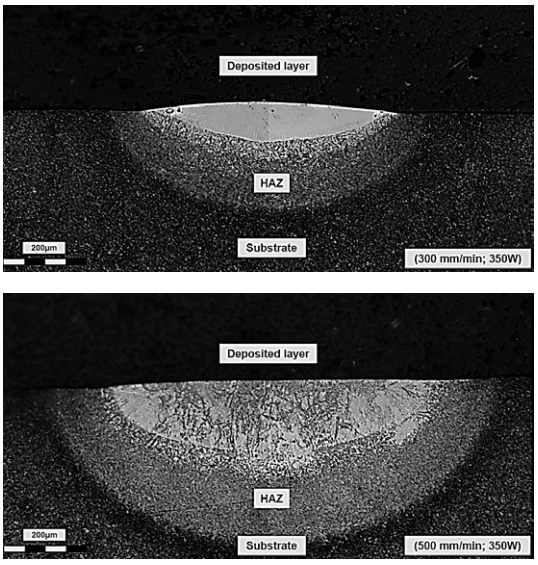

Figure 8. WC-7Ni-19Cr deposited on AISI H13 steel substrate using a power of 350 W.

Once the parameters were defined (500 mm/min-1; 250 W), a single layer was deposited using the overlapping strategy previously defined (33%) in a region of 1225 mm^2 to carry out future tests. The samples exhibit homogeneous, uninterrupted macrostructural features with no discernible surface anomalies or defects, indicative of a uniform and continuous coating process via laser cladding. It was possible to observe a thin and homogeneous deposited

layer and the heat-affected zone (HAZ) of each path traversed by the laser. In the case of the AISI H13 substrate, the region of interest exhibited a discernible presence of incompletely melted spherical powder particles, likely due to their higher mass fraction relative to the molten liquid phase during the laser cladding process. A limited number of pores and cracks were also observed in both substrates, yet did not impinge on the final quality of the coatings, as evidenced by the absence of delamination. Cross-sectional micrographs of the deposited layers, obtained using the specified parameters, are presented in Figure 10.

The surface of the WC-7Ni-19Cr coating exhibits a consistently smooth and uniform appearance, which can be attributed to both the selected overlapping pattern and the compatibility of the cladding material with the substrates. The smoothness of the deposition ensures a stable interface between the coating and substrate, which is critical under wear conditions. In the detailed cross-sectional views, the deposited layer shows a uniform and defect-free surface, in comparison, suggesting good metallurgical bonding and thermal compatibility. The transition between the deposited layer and the substrate is smooth, with minimal disturbance to the substrate microstructure in the HAZ, indicating controlled heat transfer and solidification during the cladding process. Overall, the combination of a well-selected overlapping pattern and the favorable properties of the substrates leads to a more reliable and durable coating, making it better suited for applications requiring high wear resistance.

Table 2 shows the average of microhardness results for the samples produced, with the possibility of comparing with microhardness values referring to the substrate in question. For both depositions, the deposited material showed an improvement in surface hardness, with emphasis on the deposition of WC-7Ni-19Cr on AISI 4140, which presented approximately an average microhardness value 80 % higher than the substrate value. For the AISI H13 the average microhardness value is lower, but this can be explained by have few defects that weaken the deposited layer; however, the value is similar to reported by John et al. (2022), Sun et al. (2022) and Hu et al. (2022) working with a WC cladding on 16 Mn steel (Mn—1.2 to 1.6, C—0.1 to 0.2); WC/Ni cladding on Cr12MoV steel, and WC/Ni cladding on 0Cr17Ni12Mo2 stainless steel, respectively.

Table 2. Average measurements of microhardness.

Material	Substrate	WC-7Ni-19Cr
AISI 4140	532,51 ± 34,31 HV	954,95 ± 149,01 HV
AISI H13	578,42 ± 35,51 HV	617,46 ± 61,49 HV

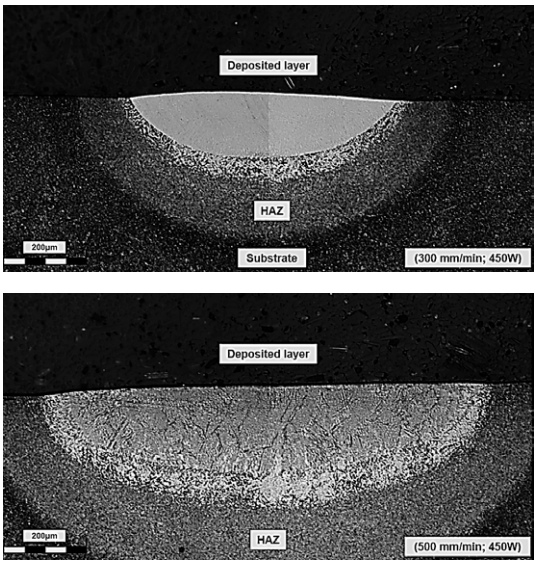

Figure 9. WC-7Ni-19Cr deposited on AISI H13 steel substrate using a power of 450 W.

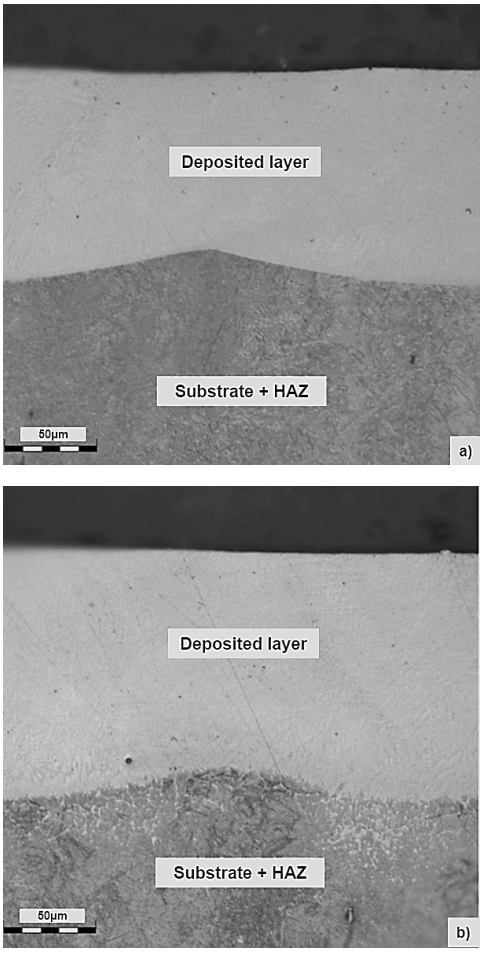

Figure 10. Detail of the WC-7Ni-19Cr layer deposited on AISI H13 (a) and AISI 4140 (b).

Vickers microhardness profiles were conducted for each sample, extending from the surface down to the substrate. Figure 11 presents the microhardness profile of a WC-7Ni-19Cr coating applied on an AISI 4140 steel substrate, illustrating the variation in hardness with increasing distance from the surface. The coating demonstrates exceptionally high surface hardness, reaching approximately 1200 HV, which is characteristic of WC-based coatings known for their excellent hardness and wear resistance due to the presence of hard tungsten carbide particles. However, a steep decline in hardness is observed within the first 200 micrometers, marking the transition into the heat-affected zone (HAZ). This reduction in hardness is attributed to the thermal exposure during the deposition process, which may result in tempering effects, microstructural alterations, or partial diffusion between the coating and substrate. Beyond the HAZ, the hardness stabilizes around 400 HV, consistent with the typical hardness of AISI 4140 steel after appropriate heat treatment, with a slight increase after 400 µm indicating some residual effects from the thermal process before reaching the unaffected region of the substrate.

High hardness of the WC-7Ni-19Cr coating underscores its effectiveness in providing superior wear resistance, which is crucial for applications involving significant abrasion or erosion. The pronounced drop in hardness within the HAZ emphasizes the necessity of controlling thermal effects during the deposition process, as an excessively large HAZ can compromise the mechanical integrity of the substrate, adversely impacting its fatigue life and wear resistance at the interface. Furthermore, the graph highlights the importance of managing the interface region between the coating and substrate, particularly within the HAZ, to ensure proper metallurgical bonding while minimizing dilution that could weaken the overall coating performance. Overall, this microhardness profile serves as a valuable tool for optimizing process parameters, ensuring that the coating delivers the desired surface hardness while mitigating adverse thermal effects on the substrate.

Figure 12 illustrates the microhardness profile of a WC-7Ni-19Cr coating applied on an H13 steel substrate, revealing the hardness behavior in relation to the distance from the surface. The hardness in the deposited layer is approximately 700 HV, which is lower than the values observed for the same coating on an AISI 4140 substrate. This difference may stem from variations in deposition conditions or microstructural interactions between the coating and the H13 steel, a tool steel recognized for its toughness and thermal resistance. In the heat-affected zone (HAZ), a more gradual decrease in hardness is noted

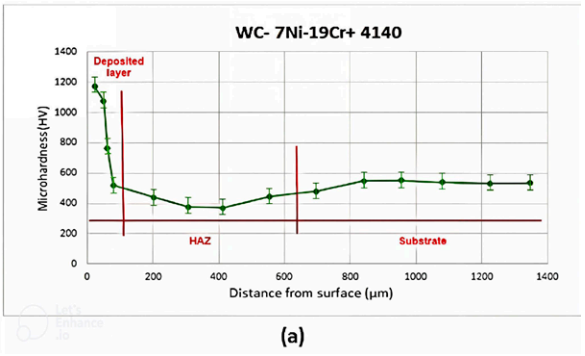

Figure 11. Vickers microhardness profile for the WC-7Ni-19Cr layer deposited on AISI 4140.

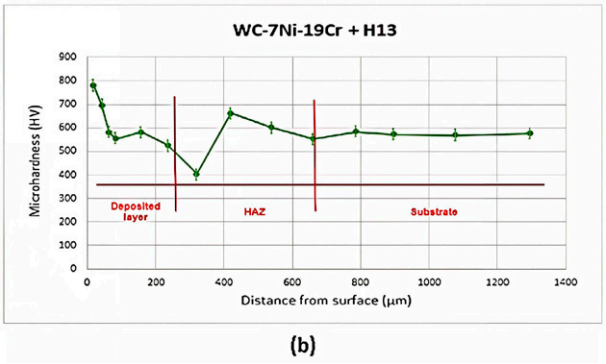

Figure 12. Vickers microhardness profile for the WC-7Ni-19Cr layer deposited on AISI H13.

as the profile transitions from the deposited layer, extending approximately 400 to 600 micrometers. This less steep decline suggests a better thermal compatibility between the coating and the H13 steel, or a more controlled diffusion zone compared to the previous data on AISI 4140.

In the substrate region, hardness stabilizes around 400 HV, which is typical for H13 tool steel after tempering. Interestingly, there is a slight increase in hardness just before reaching the substrate (around 500 to 600 µm), potentially due to re-austenitization and martensitic transformation from localized laser heating and rapid cooling. From an engineering perspective, these microhardness values demonstrate that the WC-7Ni-19Cr coating provides effective wear resistance on H13 steel, albeit slightly lower than on AISI 4140. Nevertheless, this performance remains suitable for high-stress applications, particularly where toughness and thermal stability are critical, such as in tooling and dies.

The extended HAZ and smoother hardness transition indicate that the process parameters achieved a more

uniform heat distribution, thereby reducing the risk of excessive thermal stresses. This finding suggests an optimized process for balancing coating adhesion and substrate integrity. Furthermore, the compatibility of the H13 steel substrate appears to promote better metallurgical bonding with the WC-7Ni-19Cr coating, which is evidenced by the gradual hardness variation and stable transition, potentially enhancing performance in service, particularly regarding crack resistance and wear at the interface. Overall, this microhardness profile is promising for applications demanding both wear resistance and durability under thermal cycling, making WC-7Ni-19Cr a suitable coating choice for H13 steel substrates in challenging conditions.

Figures illustrate the hardness gradient results as they transition away from the surface and the deposited layer, clearly identifying the heat-affected zone (HAZ). The microhardness values reveal a consistent trend, with the highest hardness observed in the region just below the coating surface. This phenomenon can be attributed to the rapid heating and cooling dynamics of the laser cladding process, which enhances the nucleation rate and inhibits grain growth. Consequently, this leads to grain refinement and an increased density of grain boundaries. A sharp decline in hardness values corresponds to the HAZ, where the substrate's properties are altered during processing. Beyond the HAZ, there is a normalization of microhardness values that aligns with the characteristic measurements of the substrate obtained previously. The microhardness profile measurements concluded once these values stabilized, indicating a return to the inherent hardness of the substrate. This comprehensive analysis underscores the significant effects of the laser cladding process on microhardness, particularly in terms of the gradient behavior from the surface to the substrate.

The following figures present the microadhesive wear graphs for the substrates, along with the results for the coated layers. The graphs depict the amount of material removed (in mm^3) as a function of the distance covered (in meters), corresponding to the sphere's rotations during testing. The coated layers exhibited greater wear resistance compared to the uncoated substrates, demonstrating their effectiveness in enhancing the durability of the metals used. A direct comparison of the material volume removed from the coated samples shows similar performance for the WC-7Ni-19Cr coatings on both substrates under investigation.

In Figure 13, the uncoated AISI 4140, represented by the blue curve, shows a marked increase in material removal with increasing distance, culminating in a wear track

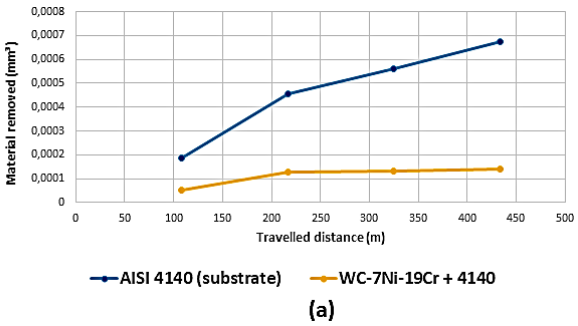

Figure 13. Results of microadhesive wear tests for WC-7Ni-19Cr coating on AISI 4140 substrate.

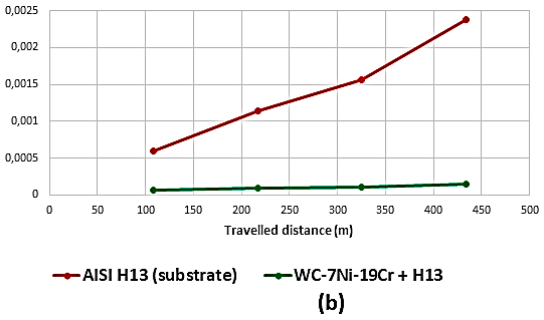

Figure 14. Results of microadhesive wear tests for WC-7Ni-19Cr coating on AISI H13 substrate.

volume of approximately 0.00055 mm^3 after 450 meters. This behavior indicates significant wear in the uncoated substrate under the test conditions. In contrast, the yellow curve, corresponding to the WC-7Ni-19Cr-coated AISI 4140, reveals a substantially lower wear rate, with minimal material removal even at greater distances—highlighting the coating's effectiveness in greatly improving the wear resistance of AISI 4140 steel.

Examining the AISI H13 substrate (Figure 14), the red curve indicates a steeper increase in material removal compared to AISI 4140, with the wear volume reaching around 0.002 mm^3 after 450 meters. This suggests that while AISI H13 is a robust tool steel, it experiences greater wear than AISI 4140 under the same conditions. However, the green curve for the WC-7Ni-19Cr coating on H13 shows minimal material removal throughout the test, remaining close to the x-axis. This indicates exceptional wear resistance provided by the coating on H13, surpassing its effectiveness on AISI 4140 and nearly eliminating wear observed in the uncoated substrate.

For the AISI H13 substrate (Figure 14), the red curve shows an even steeper increase in material removal compared to AISI 4140, with wear volume reaching

approximately 0.002 mm^3 after 450 meters. This suggests that, although H13 is a high-performance tool steel, it experiences more wear than AISI 4140 under the same test conditions. However, the green curve, representing the WC-7Ni-19Cr-coated H13, shows negligible material removal throughout the test, with values remaining close to the x-axis. This indicates an exceptional enhancement in wear resistance provided by the coating, even greater than that observed on AISI 4140, effectively eliminating the wear seen in the uncoated condition.

The influence of the substrate material is evident, as AISI H13 exhibits higher wear in its uncoated state. Nevertheless, both substrates show excellent wear resistance once coated, emphasizing the crucial role of protective layers in improving durability under frictional loads. The WC-7Ni-19Cr coating proves to be highly effective for applications exposed to high stress, friction, or abrasive environments, particularly when applied to high-strength substrates like AISI 4140 and H13. Overall, the data underscore the significant impact of WC-7Ni-19Cr coatings on improving wear performance across different steels, offering considerable advantages for use in demanding operational conditions.

The wear test results indicate that the primary wear mechanism in the uncoated substrates is microadhesive wear, characterized by progressive material loss due to localized bonding and tearing at the contact interface. This is evident in the steadily increasing wear volumes observed for both AISI 4140 and H13, with the latter displaying a higher wear rate—likely attributed to its thermal behavior and potential for microcrack formation under frictional stress. In addition to adhesion, secondary wear mechanisms such as mild abrasive wear and oxidative wear may also be present, particularly in the uncoated samples, where surface roughness or debris could accelerate material removal. In contrast, the WC-7Ni-19Cr coatings effectively suppress these mechanisms. The high hardness of the WC particles and the stable, ductile Ni-Cr matrix minimize adhesion, resist abrasion, and may assist in the formation of protective tribolayers during sliding contact. This results in significantly reduced wear rates—especially on the H13 substrate—confirming the coating's ability to mitigate multiple wear mechanisms and extend the life of metallic components.

Conclusions

The deposition of both steels in the parameter defined as ideal resulted in an increase in hardness and wear resistance. Laser cladding is a process renowned for its remarkable economic efficiency, yielding superior quality coatings on cost-effective substrates while preserving the substrate's bulk properties. The technique's exceptional performance stems from its ability to fuse metallic powders onto the substrate surface using a high-powered laser beam. The resulting coatings exhibit superior mechanical, thermal, and wear resistance properties, making them highly desirable for various industrial applications. It was established that the deposition of the WC-7Ni-19Cr coating on the tool steel (AISI H13) used as a substrate allows the improvement of properties such as hardness and wear resistance, both very important for molds and tooling where these properties are highly demanded. Similarly, by using an alloy steel (AISI 4140) widely used for the manufacture of mechanical components due to its medium mechanical strength and fracture resistance, properties such as wear resistance allow it to amplify its applications.

The process presents a promising avenue for achieving optimal material utilization, reduced production costs, and improved product quality, thus positioning it as a potential game-changer in advanced manufacturing. When tool steel (AISI H13) was used as a substrate, the intention of the deposition is to increase the interesting properties for applications of these materials, such as hardness and wear resistance, both very important for molds and tooling where these properties are highly demanded. Also, when using an alloyed steel (AISI 4140), widely used for the manufacture of mechanical components due to its medium mechanical strength and fracture resistance, it still needs properties such as wear resistance to amplify its applications. As a result, the deposition of both compositions in the parameter defined as ideal resulted in an increase in hardness and wear resistance, which demonstrates the fulfillment of the objective of the work. In this way, from the characterized coatings and the optimized process in the study, it is possible to solve very common problems of deterioration by tribological processes, providing different improved mechanical properties and improving their performance and tool life.

The experimental results obtained from the conducted tests have revealed crucial insights into the interplay between the process parameters and the resultant quality of the cladding samples. Notably, the energy density emerged as a critical factor affecting the cladding coating's performance. In the case of the composition under study, it was determined that configurations featuring a deposition velocity of 500 mm/min-1 and a power output of 250 W generated the highest quality layers, characterized by minimal or no pores, cracks, or material

detachment. Furthermore, the resulting heat-affected zone (HAZ) was relatively small, a critical consideration given the potential impact of an excessively large HAZ on the microstructure and properties of previously deposited layers. Such distortions could compromise the final product's dimensional accuracy and induce residual stresses, underscoring the importance of minimizing the HAZ in layer-by-layer construction processes.

Funding

This research was funded by the São Paulo Research Foundation (FAPESP), grant numbers 2016/11309-0 and 2019/26362-2, National Council for Scientific and Technological Development (CNPq) for funding the research process n. 305294/2015-6 and Universidad Pontificia Bolivariana, CDG-19 agreement.

Conflict of Interest

The authors declare that they have no known competing financial interests or personal relationships that could have appeared to influence the work reported in this paper. There are no conflicts of interest to disclose regarding the research, authorship, or publication of this manuscript.

References

Abijith, M. N., Nair, A. R., Aadharsh, M., Vignesh, R. V., Padmanaban, R., & Arivarasu, M. (2018). Investigations on the Mechanical, Wear and Corrosion Properties of Cold Metal Transfer Welded and Friction Stir Welded Aluminium Alloy AA2219. *Jordan Journal of Mechanical & Industrial Engineering*, *12*(4), 281. https://www.researchgate.net/profile/Vaira-Vignesh-Ramalingam/publication/337440369_Investigations_on_the_Mechanical_Wear_and_Corrosion_Properties_of_Cold_Metal_Transfer_Welded_and_Friction_Stir_Welded_Aluminium_Alloy_AA2219/links/5dd7b283299bf10c5a26dc01/Investigations-on-the-Mechanical-Wear-and-Corrosion-Properties-of-Cold-Metal-Transfer-Welded-and-Friction-Stir-Welded-Aluminium-Alloy-AA2219.pdf

Ahn, D. G. (2021). Directed energy deposition (DED) process: state of the art. *International Journal of Precision Engineering and Manufacturing-Green Technology*, *8*(2), 703-742. https://doi.org/10.1007/s40684-020-00302-7

Armstrong, M., Mehrabi, H., & Naveed, N. (2022). An overview of modern metal additive manufacturing technology. *Journal of Manufacturing Processes*, *84*, 1001-1029. https://doi.org/10.1016/j.jmapro.2022.10.060

Barragan, G. A., Mariani, F., & Coelho, R. T. (2021a). Application of 316L stainless steel coating by Directed Energy Deposition process. In *IOP Conference Series: Materials Science and Engineering* (Vol. 1154, No. 1, p. 012014). IOP Publishing. https://doi.org/10.1088/1757-899x/1154/1/012014

Barragan, G., Rojas Perilla, D. A., Grass Nunez, J., Mariani, F., & Coelho, R. (2021b). Characterization and optimization of process parameters for directed energy deposition powder-fed laser system. *Journal of Materials Engineering and Performance*, *30*(7), 5297-5306. https://doi.org/10.1007/s11665-021-05762-9

Birger, E. M., Moskvitin, G. V., Polyakov, A. N., & Arkhipov, V. E. (2011). Industrial laser cladding: current state and future. *Welding International*, *25*(03), 234-243. https://doi.org/10.1080/09507116.2010.540880

Borchers, F., Clausen, B., Eckert, S., Ehle, L., Epp, J., Harst, S., ... & Strunk, R. (2020). Comparison of different manufacturing processes of AISI 4140 steel with regard to surface modification and its influencing depth. *Metals*, *10*(7), 895. https://doi.org/10.3390/met10070895

Chen, X., Li, C., Gao, Q., Duan, X., & Liu, H. (2022). Comparison of microstructure, microhardness, fracture toughness, and abrasive wear of WC-17Co coatings formed in various spraying ways. *Coatings*, *12*(6), 814. https://doi.org/10.3390/coatings12060814

Cooke, S., Ahmadi, K., Willerth, S., & Herring, R. (2020). Metal additive manufacturing: Technology, metallurgy and modelling. *Journal of Manufacturing Processes*, *57*, 978-1003. https://doi.org/10.1016/j.jmapro.2020.07.025

Dasgupta, A., & Dutta, P. (2022). A Comprehensive Review on 3D Printing Technology: Current Applications and Challenges. *Jordan Journal of Mechanical & Industrial Engineering*, *16*(4), 529. https://jjmie.hu.edu.jo/vol-16-4/07-140-22.pdf

da Silva, D., Spinelli, J. E., Freitas, B. J. M., Mariani, F. E., Coelho, R. T., & Casteletti, L. C. (2023). Characterization of inconel and stainless steel coatings produced through directed energy deposition method using coarse powders. *Journal of Materials Engineering and Performance*, *32*(18), 8206-8216. https://doi.org/10.1007/s11665-022-07711-6

Dong, Z. H., & Fan, H. Y. (2015). Wear and morphology investigation of Cr/WC-Ni based composite coating by laser cladding. *Advanced Materials Research*, *1061*, 538-541. https://doi.org/10.4028/www.scientific.net/AMR.1061-1062.538

Du, K., Lv, Z., Fan, W., Zhang, R., Li, X., & Xu, L. (2023). Effect of heat treatment process on microstructure and mechanical properties of high-carbon H13 steel. *Processes*, *11*(11), 3239. https://doi.org/10.3390/pr11113239

Edson Mariani, F., Viana Figueiredo, G., Barragán de Los Rios, G. A., Carlos Casteletti, L., & Teixeira Coelho, R. (2023). Hardness and Wear Characteristics of Laser-Clad WC-17Co Coatings on AISI H13 and AISI 4140 Steel. *Iranian Journal of Materials Science & Engineering*, *20*(3), 1. https://doi.org/10.22068/ijmse.3206

Esteves, P. J., de Macêdo, M. C. S., Souza, R. M., & Scandian, C. (2019). Effect of ball rotation speed on wear coefficient and particle behavior in micro-abrasive wear tests. *Wear*, *426*, 137-141. https://doi.org/10.1016/j.wear.2019.01.102

Fotovvati, B., Namdari, N., & Dehghanghadikolaei, A. (2019). On coating techniques for surface protection: A review. *Journal of Manufacturing and Materials processing*, *3*(1), 28. https://doi.org/10.3390/jmmp3010028

Ghosal, P., Majumder, M. C., & Chattopadhyay, A. (2018). Study on direct laser metal deposition. *Materials Today: Proceedings*, *5*(5), 12509-12518. https://doi.org/10.1016/j.matpr.2018.02.232

Gong, N., Meng, T. L., Cao, J., Wang, Y., Karyappa, R., Ivan Tan, C. K., ... & Liu, H. (2023). Laser-cladding of high entropy alloy coatings: an overview. *Materials Technology*, *38*(1), 2151696. https://doi.org/10.1080/10667857.2022.2151696

Han, T., Zhou, K., Chen, Z., & Gao, Y. (2022). Research progress on laser cladding alloying and composite processing of steel materials. *Metals*, *12*(12), 2055. https://doi.org/10.3390/met12122055

Hu, Y., Wang, Z., & Pang, M. (2022). Effect of WC content on laser cladding Ni-based coating on the surface of stainless steel. *Materials Today Communications*, *31*, 103357. https://doi.org/10.1016/j.mtcomm.2022.103357

John, M., Kuruveri, U. B., & Menezes, P. L. (2022). Laser cladding-based surface modification of carbon steel and high-alloy steel for extreme condition applications. *Coatings*, *12*(10), 1444. https://doi.org/10.3390/coatings12101444

Kirka, M. M., Nandwana, P., Lee, Y., & Dehoff, R. R. (2017). Solidification and solid-state transformation sciences in metals additive manufacturing. *Scripta Materialia*, *135*, 130-134. https://doi.org/10.1016/j.scriptamat.2017.01.005

Mariani, E., Coelho, R. T., Silva, D., Spinelli, J. E., Juliet, B., & Freitas, M. (2022). Characterization of Inconel and Stainless-Steel Coatings Produced through Directed Energy Deposition Method Using Coarse Powders. Journal of Materials Engineering and Performance. https://doi.org/10.1007/s11665-022-07711-6

Matthews, S., Ansbro, J., Berndt, C. C., & Ang, A. S. M. (2021a). Carbide dissolution in WC-17Co thermal spray coatings: Part 1-project concept and as-sprayed coatings. *Journal of Alloys and Compounds*, *856*, 157464. https://doi.org/10.1016/j.jallcom.2020.157464

Matthews, S., Ansbro, J., Berndt, C. C., & Ang, A. S. M. (2021b). Thermally induced metallurgical transformations in WC-17Co thermal spray coatings as a function of carbide dissolution: Part 2-Heat-treated coatings. *International Journal of Refractory Metals and Hard Materials*, *96*, 105486. https://doi.org/10.1016/j.ijrmhm.2021.105486

Oladijo, O. P., Venter, A. M., & Cornish, L. A. (2014). Correlation between residual stress and abrasive wear of WC–17Co coatings. *International Journal of Refractory Metals and Hard Materials*, *44*, 68-76. https://doi.org/10.1016/j.ijrmhm.2014.01.009

Posmyk, A., & Myalski, J. (2023). Coatings protecting against aviation piston engine seizure. *Wear*, *518*, 204627. https://doi.org/10.1016/j.wear.2023.204627

Santo, L. (2008). Laser cladding of metals: a review. *International Journal of Surface Science and Engineering*, *2*(5), 327-336. https://doi.org/10.1504/IJSURFSE.2008.021345

Shamsaei, N., Yadollahi, A., Bian, L., & Thompson, S. M. (2015). An overview of Direct Laser Deposition for additive manufacturing; Part II: Mechanical behavior, process parameter optimization and control. *Additive manufacturing*, *8*, 12-35. https://doi.org/10.1016/j.addma.2015.07.002

Singh, S., Ramakrishna, S., & Singh, R. (2017). Material issues in additive manufacturing: A review. *Journal of Manufacturing Processes*, *25*, 185-200. https://doi.org/10.1016/j.jmapro.2016.11.006

St-Georges, L. (2007). Development and characterization of composite Ni–Cr+ WC laser cladding. *wear*, *263*(1-6), 562-566. https://dio.org/10.1016/j.wear.2007.02.023

Sun, W., Zhang, D., Chen, X., Wang, K., Zhang, J., & Jia, Y. (2022). Effect of the scanning speed of laser cladding on microstructure and mechanical properties of WC/Ni composite coatings. *Journal of Mechanical Science and Technology*, *36*(2), 679-687.
https://doi.org/10.1007/s12206-022-0115-9

Svetlizky, D., Das, M., Zheng, B., Vyatskikh, A. L., Bose, S., Bandyopadhyay, A., ... & Eliaz, N. (2021). Directed energy deposition (DED) additive manufacturing: Physical characteristics, defects, challenges and applications. *Materials today*, *49*, 271-295.
https://doi.org/10.1016/j.mattod.2021.03.020

Thompson, S. M., Bian, L., Shamsaei, N., & Yadollahi, A. (2015). An overview of Direct Laser Deposition for additive manufacturing; Part I: Transport phenomena, modeling and diagnostics. *Additive Manufacturing*, *8*, 36-62.
https://doi.org/10.1016/j.addma.2015.07.001

Tougherghi, F., Ahnia, F., Khenfer, K., Miroud, D., Zaid, B., Yaşar, M., & Khoshnaw, F. (2022). Microstructure, tribological, and electrochemical characterization of hardfacing WC-Ni-Cr on AISI 1045 carbon steel alloy. *Journal of Materials Engineering and Performance*, *31*(9), 7641-7652.
https://doi.org/10.1007/s11665-022-06781-w

Toyserkani, E., Khajepour, A., & Corbin, S. (2017). Laser Cladding. In New York (Vol. 11, Issue 2).

Van Acker, K., Vanhoyweghen, D., Persoons, R., & Vangrunderbeek, J. (2005). Influence of tungsten carbide particle size and distribution on the wear resistance of laser clad WC/Ni coatings. *wear*, *258*(1-4), 194-202.
https://doi.org/10.1016/j.wear.2004.09.041

Wang, T., Zhu, L., Song, H., & Wang, H. (2022). Effect of WC-17Co content on microstructure and properties of IN718 composites prepared by laser cladding. *Optics & Laser Technology*, *148*, 107780.
https://doi.org/10.1016/j.optlastec.2021.107780

You, A., Wang, N., Chen, Y., Jiang, C., Zhang, Y., Zhao, Q., ... & Zhao, Y. (2023). Effect of linear energy density on microstructure and wear resistance of WC-Co-Cr composite coating by laser cladding. *Surface and Coatings Technology*, *454*, 129185.
https://doi.org/10.1016/j.surfcoat.2022.129185